Electronic Supplementary Material (ESI) for RSC Advances.

SUPPORTING INFORMATION

Unprecedented Inhibition of Glycosidase-Catalyzed Substrate Hydrolysis by Nanodiamond-Grafted *O*-Glycosides

Aloysius Siriwardena, Manakaman Khanal, Alexandre Barras, Omprakash Bande, Teresa Mena-Barragán, Carmen Ortiz Mellet,* José Manuel Garcia Fernàndez,* Rabah Boukheroub, and Sabine Szunerits**

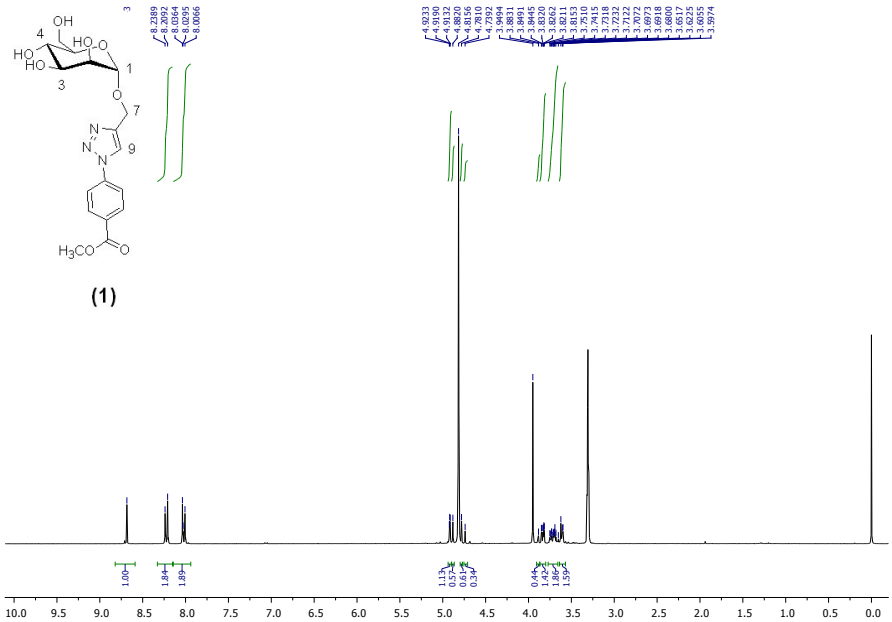

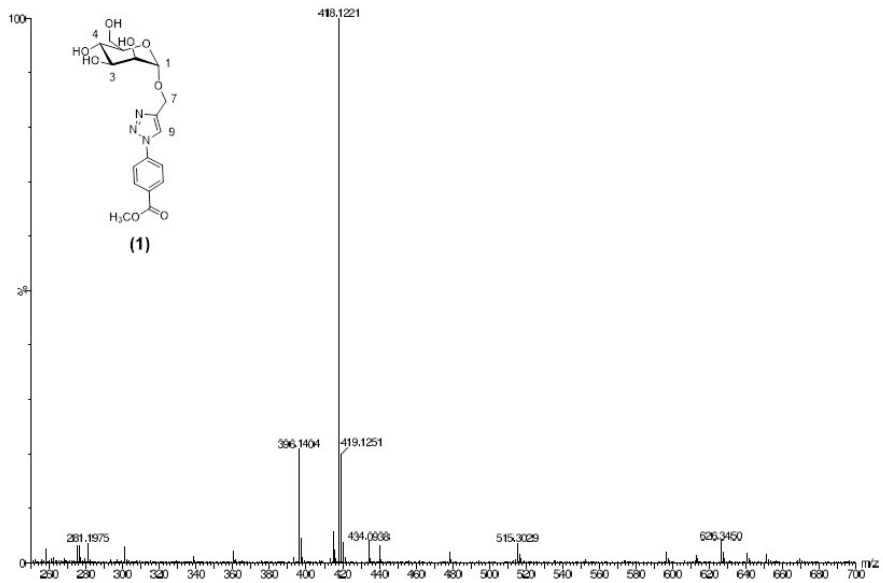

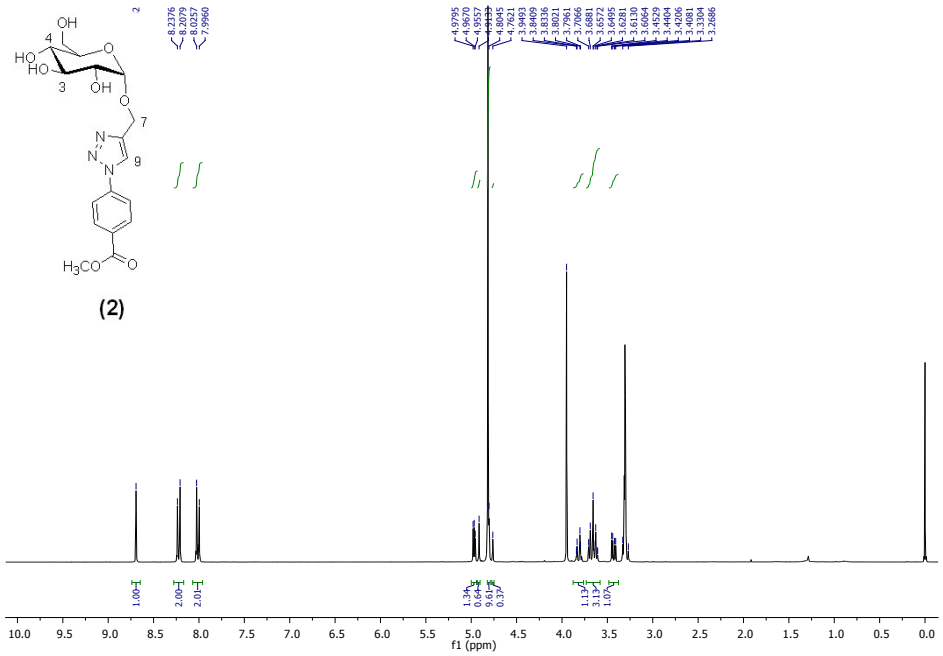

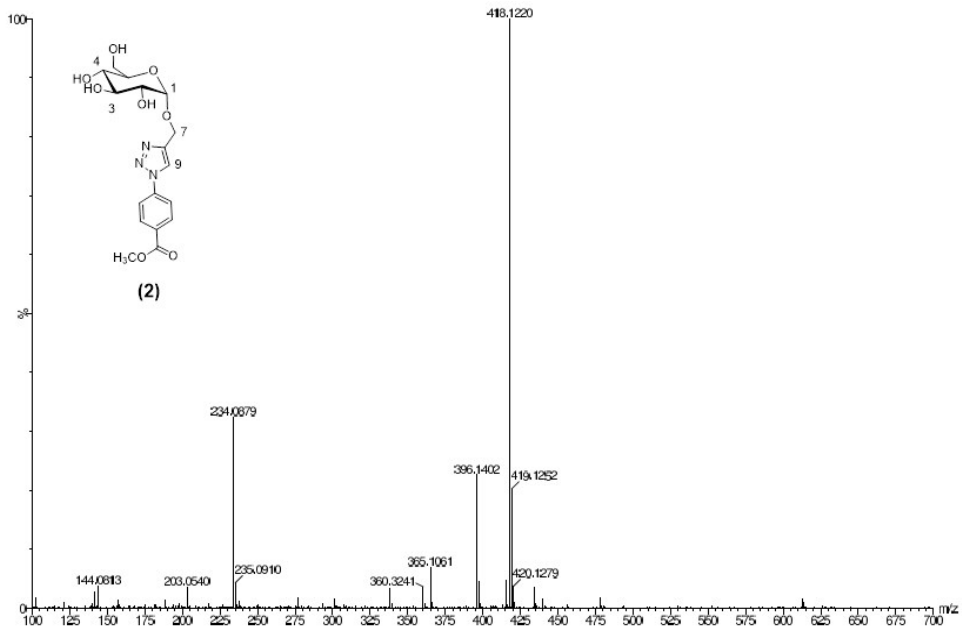

Figure S1: [1]HNMR (300 MHz, CD3OD) Spectra & HRMS for Compounds (**1**) and (2)

The formed particle were characterised by Fourier transform infrared (FT-IR) spectroscopy (**Figure S1A**) by X-ray photoelectron spectroscopy (XPS) (**Figure S1B**). In the case of FT-IR analysis, ND-OH particles show a broad peak at 3400 cm^{-1} assigned to the vibration of surface hydroxyl groups or/and adsorbed water molecules, and an additional sharper one at 1633 cm^{-1} due to the bending mode $\delta_{(OH)}$ of surface hydroxyl groups on the NDs. In addition, the band at 1107 cm^{-1} is indicative of the presence of C-O-C- functions of cyclic ethers. The FTIR spectrum of the ND-N_3 particles displays a band at 2125 cm^{-1} characteristic of the $\nu_{as(N3)}$ stretching mode, a broad peak at 3447 cm^{-1} assigned to the stretching mode of unreacted surface hydroxyl groups or/and adsorbed water molecules and a band at 2936 cm^{-1} characteristic of the presence of C-H bonds. The band at 1730 cm^{-1}, (C=O) confirms the formation of an ester linkage, while the band at 1286 cm^{-1} can be attributed to C-O bond stretching on the ND surface. Successful "clicking" of any propargylated partner to the ND-N_3 surface results in the consumption of azide functions and their replacement with surface triazole groups. As a consequence the $\nu_{as(N3)}$ stretching mode at 2123 cm^{1} is absent in the FT-IR spectra of clicked products.

The high-resolution N1s XPS spectra of ND-N_3 particles reveals unambiguously, the presence of the azido function by the signals at 405.2 (Ar-N=$\underline{N}^{+}$=N^{-}) and 401.6 eV (Ar $\underline{N}$=N^{+}=$\underline{N}^{-}$) in a ratio of 1:2, as theoretically expected. The bands at 399.3 and 402.4 eV with a ratio of 3:1 correspond to C-N and N-O bands present in the initla ND-OH particles. The conversion of the surface azide groups into the corresponding triazole functions is seen by the absence of the characteristic azide band at 405.2 eV, and by the prescene of banda at 402.6 eV (-C-N-) and 400.4 eV (-N=N-) respectively, typical of a triazole functions.

A representative transmission electron microscopy (TEM) images of the different diamond nanostructures (**Figure S1C**) reveal the presence of spherical particles with a mean diameter of 12 ± 4 nm for all structrues independent of the sugar present.

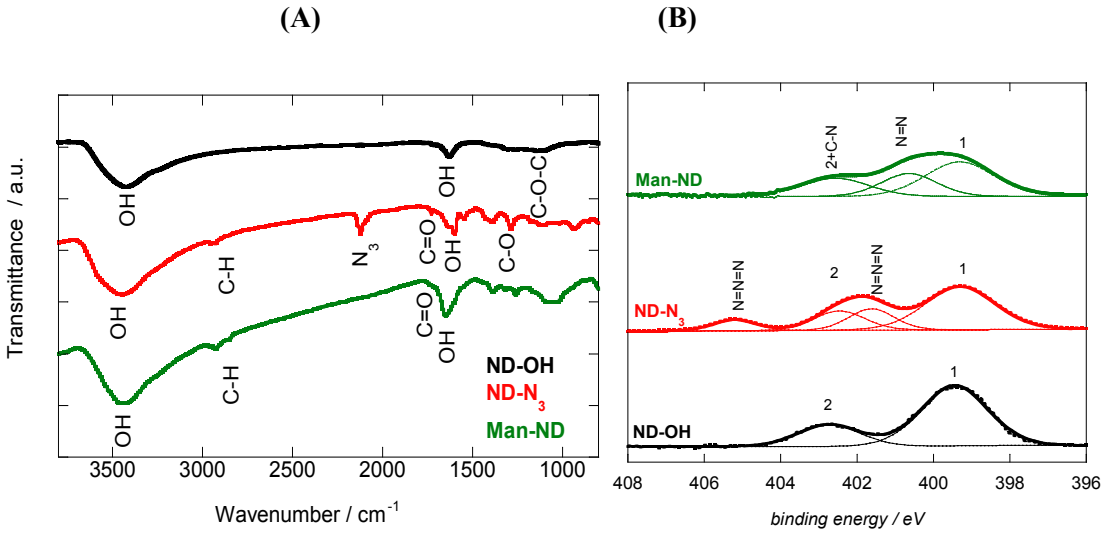

(C)

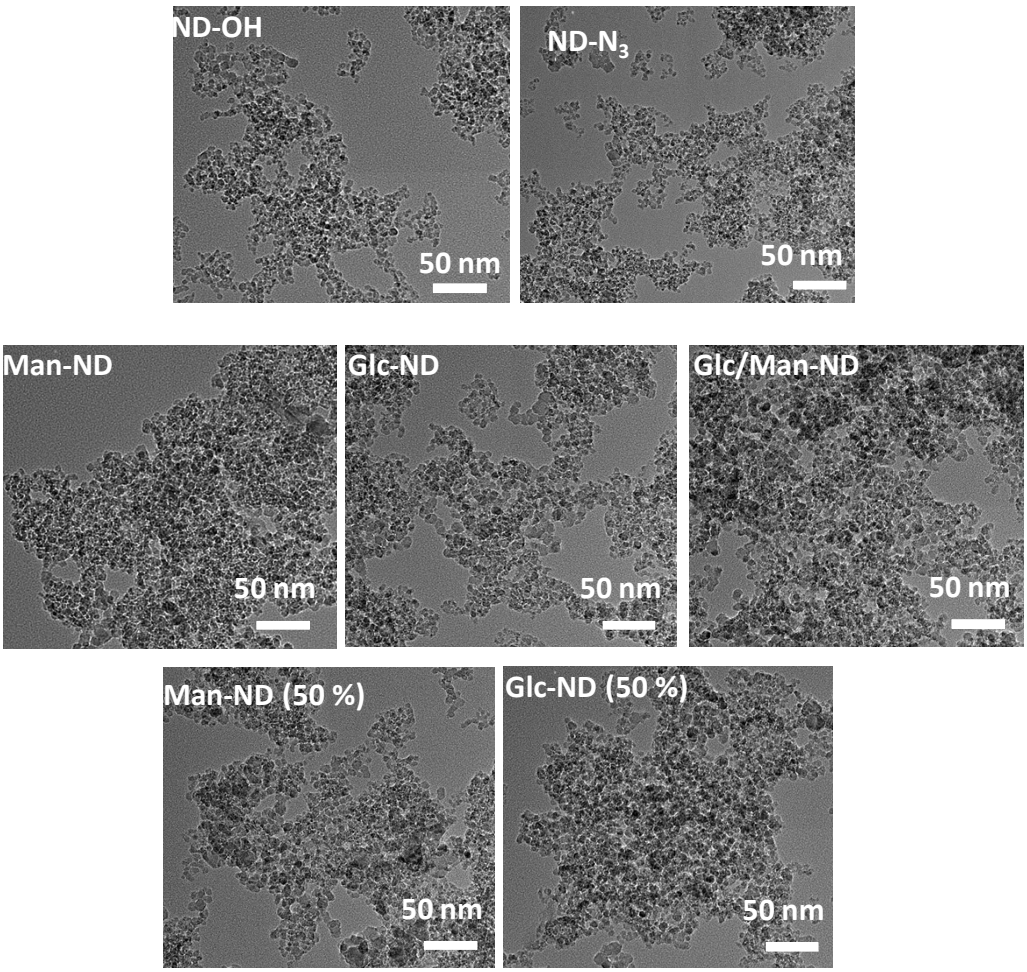

Figure S2. FT IR (A), and XPS spectra (B) of ND-OH (black), ND-N_3 (red) and Man-ND (green) ; (C) TEM images of ND-OH, ND-N_3, Man-ND, Glc-ND, Glc/Man-ND, Man-ND (50 %), Glc-Nd (50 %)

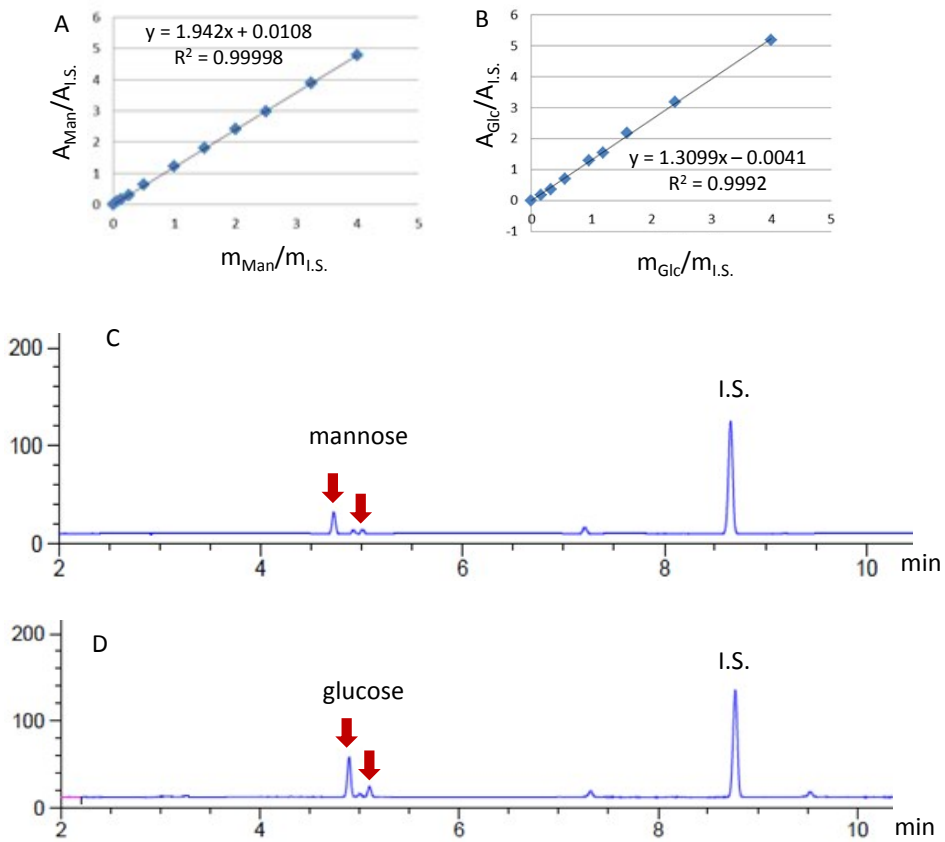

Figure S3: A) Calibration plot for mannose. B) Calibration plot for glucose. C) Representative example of chromatograms obtained after incubation of (**1**) with α-mannosidase. Representative example of chromatograms obtained after incubation of (**2**) with maltase. I.S. is the internal standard (phenyl β-D-glucopyranoside).

The plots of the relative amounts of bound ConA-HRP as a function of glyco-ND concentration are presented in **Figure S3**, with the maximum for the Man-ND at the higher concentration (150 μM) set at 100 %. Relative crosslinking efficiencies at this concentration are also shown shown. The crosslinking ability of the Man-ND and Man-ND (50 %) was approximately three-fold and twice respectively, that of the corresponding Glc-ND of equivalent sugar content. Glc/Man-ND particles are seen to be much more efficient than either Man-ND (50 %) or Glc-ND (50 %) and almost as efficient as Man-ND. To check whether or not the observed reinforcing of the cross-linking potential arises from the interplay of different bridging mechanisms involving preferentially the mannopyranosyl and the glucopyranosyl ligands, a control experiment was performed using Glc-ND and Man-ND at concentrations of 75 μM each. The relative cross-linking value obtained (41%) is virtually identical to that of pure Man-ND at 75 μM (39%), strongly suggesting that the enhanced cross-linking potential of the mixed Glc/Man- ND is a consequence of an increased ConA binding affinity for the heteroligand system and requires that both glycotopes be simultaneously exposed on the surface of the ND particles.

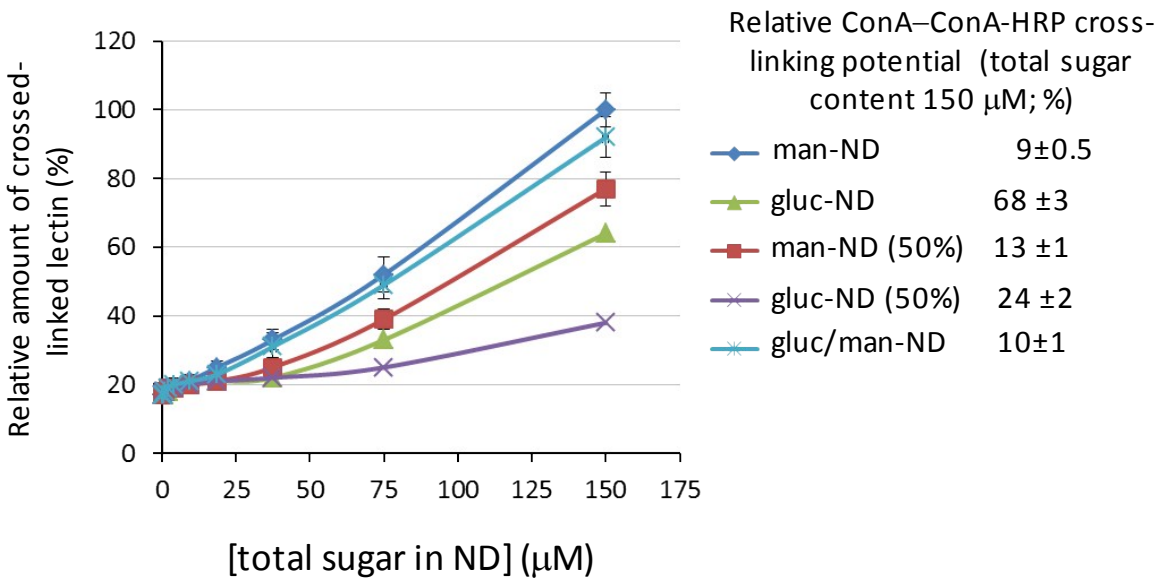

Figure S4. Two-site sandwich ELLA: Plots of the relative crosslinking efficiencies of the various glyco-ND at different concentrations in sugar basis (mean of three independent experiments ±SD). The corresponding values at the highest assayed concentration (150 μM) are given corrected for background (18±1%).

Many signalling events are dependent on the rate of ligand binding and the rate of multivalent ligand-induced receptor clustering. To test whether the differences in simultaneously binding two ConA lectin molecules by

the glyco-ND as a function of the glycotope motif and the sugar content correlated with their relative capacity to promote the formation of three-dimensional aggregates, a kinetic turbidimetry assay was carried out. Turbidity measurements can be used to monitor the formation of cross-linked complexes in real time. For that purpose, the glyco-ND (50 μL) at the appropriate concentration in PBS were added to a solution of ConA (50 μL; 1 mg mL^{-1} in PBS pH 7.3, containing 0.1 mm Ca^{2+} and 0.1 mm Mn^{2+}). The time-dependent turbidity kinetics was recorded by measuring the absorption coefficient at 490 nm at intervals of 1 min for 35 min.

At concentrations of over 50 μM (sugar basis content), lectin aggregation occurred, in all cases, too rapidly to allow a comparative evaluation. This observation is idicative that the glyco-ND platform promotes 3D-network formation with high efficiency. Time course measurements were conducted at concentrations of 37.5, 18.7 and 9.3 μM (**Figure S5, A-C**). The initial rate of precipitation (V_i) was determined through linear fitting of the initial portion of the data (**Figure S5, D**). In accordance with their relative ConA binding affinities, the manno-ND are seen to induce more rapid lectin aggregation than the corresponding gluco-ND with equivqlent sugar loading. Somewhat surprisingly, Glc/Man-ND exhibited the highest precipitation rate under all conditions investogated, implying that the amalgamation of glucopyranosyl and mannopyranosyl glycotopes favours kinetic lectin crosslinking.

The stability of the ConA—glyco-ND networks was also assessed by comparing the ability of mannose, a competitive monovalent Con A lectin ligand, to disrupt the aggregates (clear solutions). After 15 min, mannose (100 mM, 100 μL) was added to each network suspension so as assure respectively, 2500-, 5000- and 10.000-fold mannose concentrations relative to the ND-cnjugated sugar content. Full reversion of the aggregated networks was observed in all experiments with homogeneous Glc-ND. However, the aggregates formed from Man-ND at 37.5 and 18.7 μM, either homogeneous or heterogeneous, partially resisted mannose-induced disruption after the initial addition and required addition of a second aliquot of mannose (shown after 25 min in **Figure S5 (A-C**) to afford completely clear solutions. Thus, the Man-ND network exhibited a far higher stability than that formed from Glc/Man-ND, in spite of the reversed order encountered for aggregation rates, further highlighting the potential of secondary glycotopes to modulate the properties of lectin ligands in a multifactorial manner.

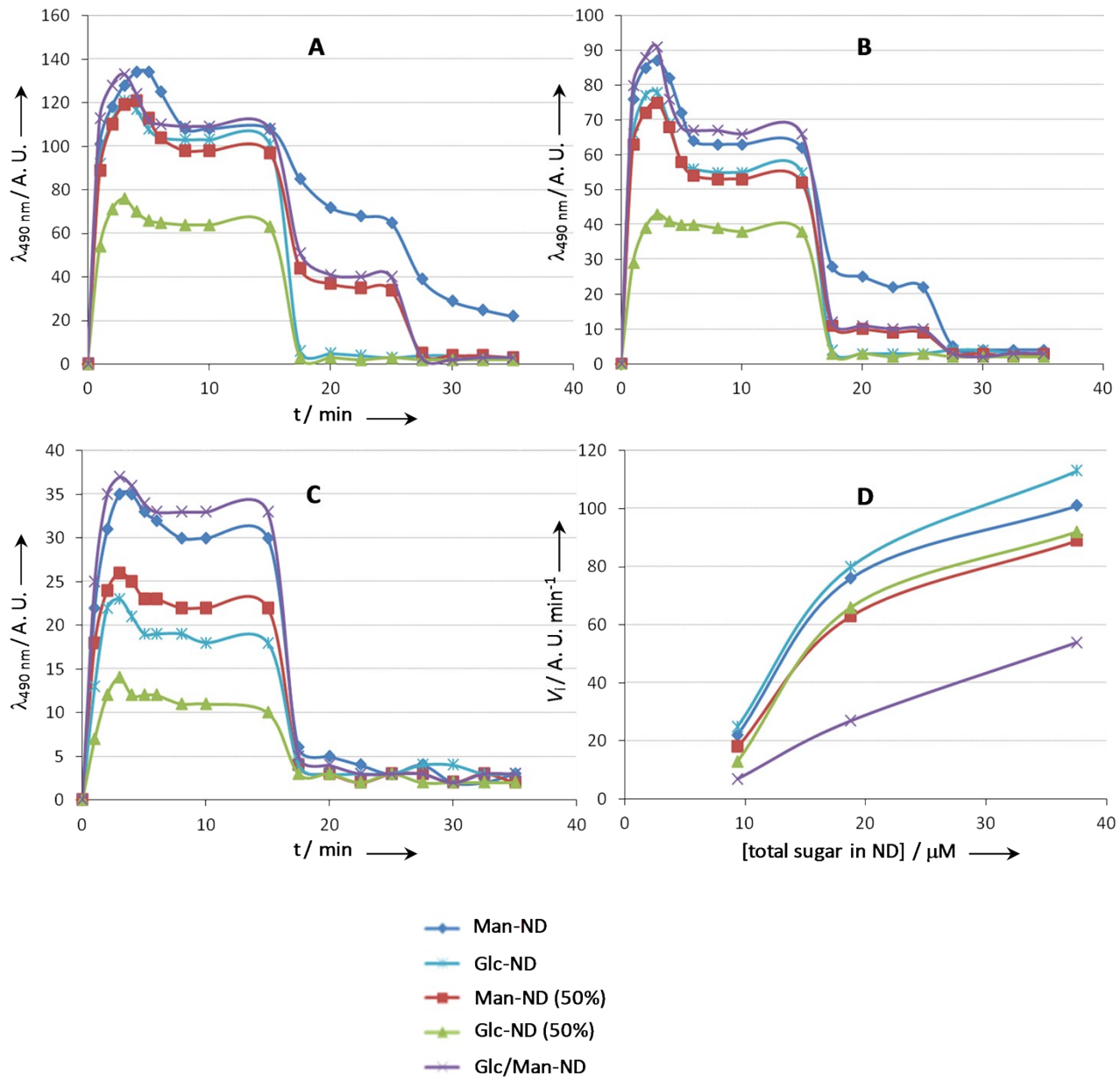

Figure S5. Turbidity assay: Absorption changes measured for ConA (1 mg mL^{-1}) at 490 nm upon addition of each of the glyco-NDs at either 37.5 (A), 18.7 (B) or 9.4 µM (C) in sugar basis. α-D-Mannose (100 mM) was added to all mixtures after 15 min and again after 25 min. The initial aggregation rates (*Vi*) at each concentration, derived from linear fits of the initial portion of the curves, are also shown (D).

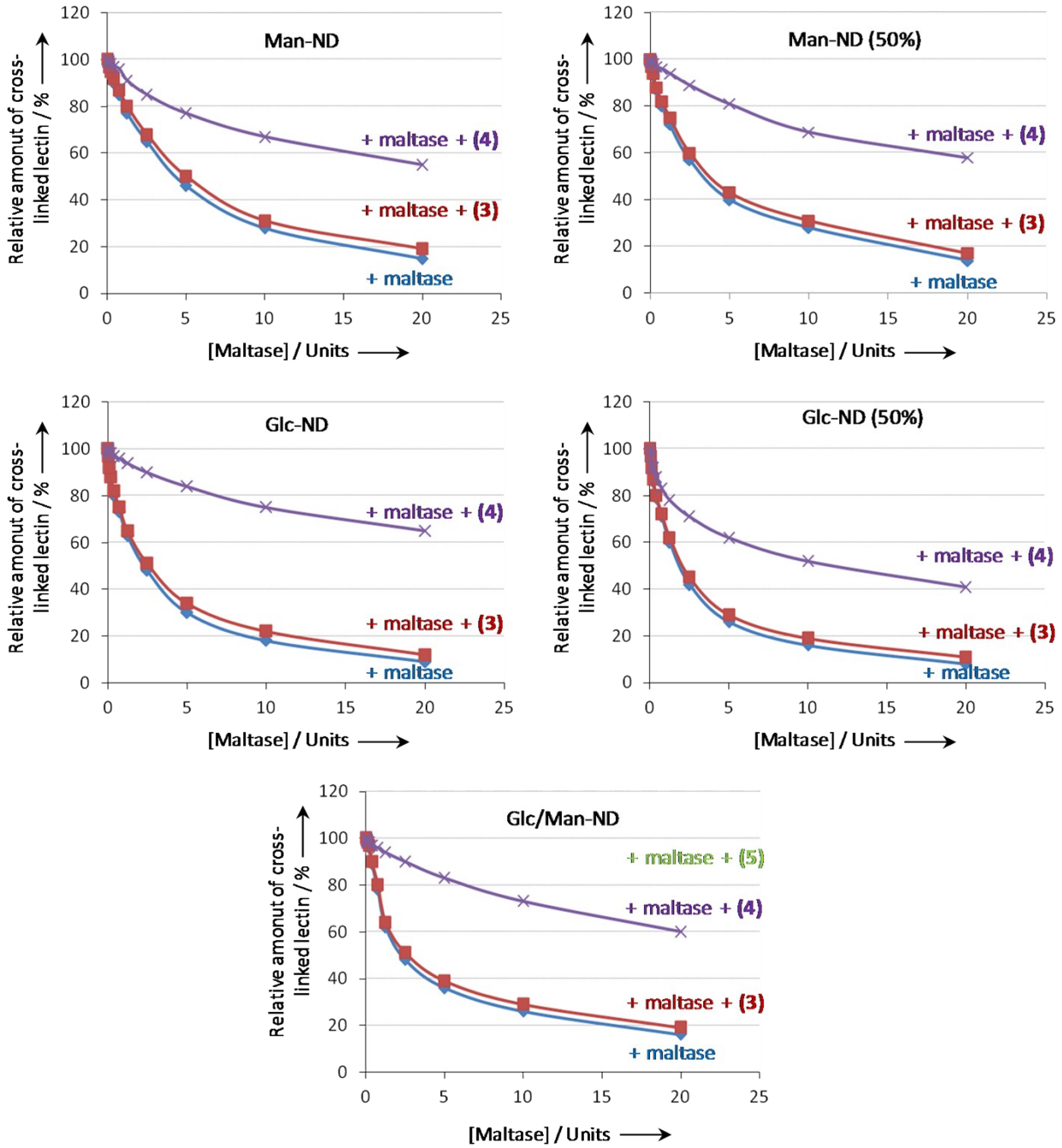

Figure S6. Plots of the inhibition of the ConA—ConA-HRP cross-linking mediated by the various glyco-NDs in the two-site ELLA tests with increasing amounts of maltase. Data have been collected in the absence and in the presence of an excess of either the monosaccharide analogue inhibitor (**3**) or the isomaltase analogue inhibitor (**4**) and represent the mean of three independent determinations (SD 12-18%).